



# DoD CORROSION CONFERENCE 2011

DoD 2011-20721

## Corrosion Inhibition of AA2024-T3 by Aqueous Molybdate, Silicate, and Praseodymium Species



Omar Lopez-Garrity and G.S. Frankel  
The Ohio State University, Fontana Corrosion Center  
477 Watts Hall, 2041 College Road  
Columbus, Ohio, 43210

### ABSTRACT

The mechanism of corrosion inhibition of aluminum alloy 2024-T3 by silicate, molybdate, and praseodymium was investigated using standard electrochemical techniques and *in situ* atomic force microscopy (AFM) scratching. The latter technique is used to analyze the early stages of corrosion at selected sites with sub-microscopic resolution. Furthermore, free corrosion tests coupled with SEM analysis were performed on samples immersed in aerated solution with and without inhibitor. All inhibitors reduced the corrosion rate of AA2024-T3. The order of ascending inhibiting potency among the inhibitors tested is molybdate < silicate < praseodymium.

Keywords: AA2024-T3, aluminum alloys, corrosion inhibition, sodium silicate, sodium molybdate, praseodymium chloride.

### INTRODUCTION

High strength AA2024-T3 is commonly employed in aircraft structure and design. Its mechanical properties are attributed to the addition of alloying elements such as Cu, Mg, Fe, and Mn, which segregate to form intermetallic particles. However, the resulting heterogeneous microstructure increases the susceptibility to localized corrosion in the form of pitting, intergranular, exfoliation, and filiform corrosion. Therefore, multi-layered coating protection schemes involving conversion coatings and pigments have been used to mitigate corrosion of aerospace aircraft. These systems release soluble inhibiting species into the local environment, suppressing corrosion either through anodic or cathodic inhibition. The objective of this work is to understand the mechanism of corrosion inhibition of selected nonchromate soluble species, namely silicate ( $\text{SiO}_3^-$ ), molybdate ( $\text{MoO}_4^{2-}$ ) and praseodymium ( $\text{Pr}^{3+}$ ), for AA2024-T3. This information should assist development of non-chromate protection schemes that offer the same level of robustness and reliability as chromate systems. The approaches taken include standard electrochemical experiments, SEM-EDS analysis of coupons immersed in bulk solution, and *in situ* atomic force microscopy (AFM) scratching to evaluate the corrosion kinetics in the presence of inhibiting ions. The latter technique involves generating sub-microscopic topographical images of the chronological sequence of attack during *in situ* scratching at the open-circuit potential (OCP).

## EXPERIMENTAL PROCEDURE

Samples of AA2024-T3 (3.9-4.9% Cu, 1.2-1.8% Mg, 0.3-0.9% Mn, 0.5% Fe, 0.5% Si by weight) were mechanically polished to 1200 grit SiC in a nonaqueous slurry to minimize the onset of corrosion. Samples analyzed with AFM, SEM, and XPS were further polished to 1  $\mu\text{m}$  diamond paste. All samples were cleaned with ethanol in an ultrasonic bath, air dried, and stored overnight in a desiccator. Cyclic polarization curves were performed under deaerated conditions to study the passivation and repassivation kinetics of the working electrode. Cathodic polarization experiments were performed under quiescent aerated conditions. A scan rate of 0.167 mV/sec was used for all tests starting at OCP.

*In situ* AFM scratching experiments were performed with a Veeco Multimode AFM coupled with a Nanoscope 7 controller. Electrolyte was introduced into a special 10 ml glass cell at a rate of 10 ml/h using a peristaltic pump. Scratching was performed in contact mode with a Si cantilever tip. In contact mode, the tip deflection is kept constant at a force that is set by a user-controlled parameter, the set point (SP) potential. The SP is representative of the photodiode potential and ranges between -0.5 to 10 V, which represents forces of about 100 to 500 nN. However, the tip pressure can change because geometrical alterations occur at the tip during scratching, therefore forces are reported in terms of SP only. The interactional force between the tip and the surface is proportional to the SP; increasing the SP from low to high value increases the force applied on the surface by the tip. Tips were replaced after each experiment due to wear from hydrogen gas evolution and other corrosion products that form during scratching. Furthermore, scan rates were held constant at 2 Hz, which results in a capture time of 4 to 5 minutes per scan.

## RESULTS AND DISCUSSION

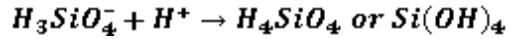
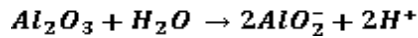
### Sodium Silicate

The natural pH of solution containing 1 mM or 10 mM silicate is equal to 10.9 or 11.9, respectively. The most significant effect of the polarization experiments is that silicate reduces the passivation current density by 1.5 orders of magnitude in 1 mM concentration. At 10 mM, this effect is not as large, which can be explained by the higher solution pH, which results in a more aggressive solution. Furthermore, it can be observed from cathodic polarization that the OCP shifts from -1200 to -550 mV SCE with the addition of silicate. These results indicate that sodium silicate imparts protection by significantly increasing passivity on the surface. This would explain the increase in OCP observed during cathodic polarization. Hydrogen evolution rate is also decreased in the presence of silicate. XPS conducted on a sample exposed to silicate solution after 48 hours reveals a significant increase in Si concentration and the presence of a thicker oxide on the surface.

AA2024-T3 coupons immersed in 0.1 M NaCl solution with sodium silicate in as-prepared solution (pH 11) exhibited attacked S-phase particles (Al-Cu-Mg) were enriched in Cu and Si, and depleted in Mg. Si may have precipitated in pits in the form of silica (i.e.  $\text{SiO}_2$ ) as a result of a decreased pH associated with metal hydrolysis inside the pit.

AFM scratching in 1 mM sodium silicate resulted in S-phase particle attack after scratching for low SP for 3 hours. After increasing the SP to larger values, pitting was observed on the matrix. Furthermore, no trenching was observed around the remaining particles including the noble Fe-Mn containing IMCs. *Ex situ* EDS analysis revealed Cu-enriched S-phase particles did suffer removal from matrix. Si was also detected inside attacked S-phase particles, again probably due to precipitation of silica inside the pit resulting from metal hydrolysis. In-solution without inhibitor, S-phase particles were completely removed from the surface and trenching around a large IMC was observed after 30 minutes of scratching at 0.5 V SP. It should be noted that in chromate and vanadate containing solutions, corrosion attack nucleated after scratching for 6 to 8 hours at significantly higher SPs.

Based on these results, a mechanism for the corrosion inhibition by silicate is proposed; in alkaline solutions, naturally occurring aluminum oxide dissolves into aluminate (i.e.  $\text{AlO}_2^-$ ). Following this, silicate may improve passivity by forming a thin-layer of silicon-hydroxide by,



Furthermore, the detection of Si inside the pits suggests that silicate precipitates preferentially at defect sites and may block further attack. At low pH (details not given), aluminum dissolution appears to promote the deposition of insoluble aluminum silicate over the whole surface. As the film thickens, it may provide passive corrosion inhibition by blocking the access of electrolyte to the metal substrate. This, however, is a slow process. AFM results show that silicate reduces the dissolution rate of AA2024-T3; attack was observed around a large IMC after 3 hours of scratching at 1 V SP and no other particle was completely dissolved away.

### Sodium Molybdate

The natural pH of molybdate-containing solution was measured to be 7.8. Anodic polarization showed that molybdate imparted anodic inhibition by increasing the pitting potential by 100 mV at 10 mM concentration. The passive current density on the reverse scan also increased. Cathodic polarization reveals that molybdate increased the OCP, which was pinned at the pitting potential. However, the cathodic limiting current density also increased. Interesting electrochemical behavior was observed at pH 5. Cathodic polarization in deaerated solution containing 10 mM molybdate increased the cathodic limiting current density. In addition, anodic polarization revealed no passive region. These results indicate that at pH 5 molybdate reduces in a fashion that is not self-inhibiting resulting in accelerated corrosion. Poor corrosion inhibition by molybdate in acidic media may result from the polymerization of molybdate species that render poor inhibition.

AFM scratching in 0.5 M NaCl solution containing 10 mM Na<sub>2</sub>MoO<sub>4</sub> resulted in attack around the periphery of a large IMC after 1 hour of scratching at 0 V SP. In comparison, scratching in 0.5 M NaCl solution only resulted in attack after 20 min of scratching at this same SP. Molybdate clearly does not perform well in inhibiting corrosion of AA2024-T3.

### Praseodymium Chloride

The natural pH of praseodymium containing solution was measured to be around 5.6. Potentiodynamic measurements at varying praseodymium concentrations in 0.1 M NaCl background solution showed a 2 order of magnitude decrease in oxygen reduction kinetics. In addition, virtually no change in OCP was observed. Anodic polarization revealed a decrease in anodic current density above the first breakdown potential associated with S-phase particle dissolution. Optimum inhibition was observed with an inhibition concentration of 50 ppm. Furthermore, SEM analysis of a sample immersed in praseodymium-containing solution revealed the presence of an oxide film over S-phase particles, characterized as praseodymium hydroxide. Interestingly, no significant amount of oxide was present over the more noble Fe-Mn containing IMCs.

AFM scratching in praseodymium containing solution resulted in no attack until the SP was raised to intermediate values at which point trenching was observed around the periphery of all IMCs. *Ex situ* SEM analysis of the scratched area revealed that both S-phase and Fe-Mn IMCs were still intact. Based on these results, it is concluded that the order of ascending inhibiting potency among the inhibitors tested is molybdate < silicate < praseodymium. However, none performed as well as chromate, or even vanadates, which were tested in past studies.

## CONCLUSIONS

All inhibitors reduced the corrosion rate of AA2024-T3. Silicate inhibited the anodic kinetics, enhancing passivity. Molybdate shifted the pitting potential to nobler potentials in near-neutral solutions, while rendering poor inhibition at low pH. Praseodymium reduced the oxygen reduction kinetics, thereby

significantly reducing the corrosion rate. The order of ascending inhibiting potency among the inhibitors tested is molybdate, silicate, and praseodymium. However, none performed as well as chromate, or even vanadates, which were tested in past studies.

### **ACKNOWLEDGEMENTS**

The authors would like to acknowledge Dr. Saikat Adhikari for his AFM assistance. The authors would also like to thank the Strategic Environmental Research and Development Program (SERDP) for funding this project.